CORA Cork Open Research Archive
Cartlann Taighde Oscailte Chorcaí

Title	NiVO3 fused oxide nanoparticles - an electrochemically stable intercalation anode material for lithium ion batteries
Authors	McNulty, David;Collins, Gillian;O'Dwyer, Colm
Publication date	2018-08-28
Original Citation	McNulty, D., Collins, G. and O'Dwyer, C. (2018) 'NiVO3 fused oxide nanoparticles - an electrochemically stable intercalation anode material for lithium ion batteries', Journal of Materials Chemistry A. doi:10.1039/C8TA05327H
Type of publication	Article (peer-reviewed)
Link to publisher's version	10.1039/C8TA05327H
Rights	© 2018, the Authors. Published by the Royal Society of Chemistry. All rights reserved. This is the Accepted Manuscript of an article published in Journal of Materials Chemistry A on 28th August, 2018, available online: https://dx.doi.org/10.1039/C8TA05327H
Download date	2026-11-05 22:03:34
Item downloaded from	https://hdl.handle.net/10468/6747

UCC
University College Cork, Ireland
Coláiste na hOllscoile Corcaigh

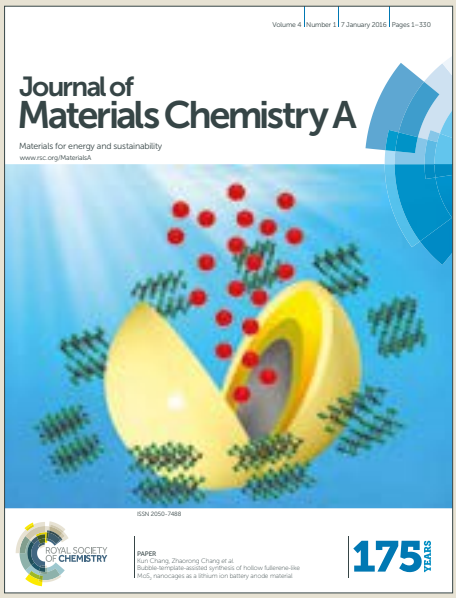
Check for updates

View Article Online
View Journal

Journal of Materials Chemistry A

Accepted Manuscript

This article can be cited before page numbers have been issued, to do this please use: D. McNulty, G. Collins and C. O'Dwyer, *J. Mater. Chem. A*, 2018, DOI: 10.1039/C8TA05327H.



This is an Accepted Manuscript, which has been through the Royal Society of Chemistry peer review process and has been accepted for publication.

Accepted Manuscripts are published online shortly after acceptance, before technical editing, formatting and proof reading. Using this free service, authors can make their results available to the community, in citable form, before we publish the edited article. We will replace this Accepted Manuscript with the edited and formatted Advance Article as soon as it is available.

You can find more information about Accepted Manuscripts in the author guidelines.

Please note that technical editing may introduce minor changes to the text and/or graphics, which may alter content. The journal's standard Terms & Conditions and the ethical guidelines, outlined in our author and reviewer resource centre, still apply. In no event shall the Royal Society of Chemistry be held responsible for any errors or omissions in this Accepted Manuscript or any consequences arising from the use of any information it contains.

ROYAL SOCIETY OF CHEMISTRY

rsc.li/materials-a

$NiVO_3$ Fused Oxide Nanoparticles – An Electrochemically Stable Intercalation Anode Material for Lithium Ion Batteries

View Article Online
DOI: 10.1039/C8TA05327H

David McNulty[a], *Gillian Collins*[a,b] *and Colm O'Dwyer*[a,c,d*]

[a]School of Chemistry, University College Cork, Cork T12 YN60, Ireland
[b]CRANN@AMBER, Trinity College Dublin, Dublin 2, Ireland
[c]Micro-Nano Systems Centre, Tyndall National Institute, Lee Maltings, Cork T12 R5CP, Ireland
[d]Environmental Research Institute, University College Cork, Lee Road, Cork T23 XE10, Ireland
*Email - c.odwyer@ucc.ie

Published on 28 August 2018. Downloaded by University College Cork on 9/6/2018 9:15:37 AM.

Journal of Materials Chemistry A Accepted Manuscript

Abstract

For oxides, especially as lithium-ion battery anodes, it is important to engineer the material not only to improve kinetics of reversible lithiation efficiency, but to avoid capacity and voltage fading, and side reactions, from conversion modes processes that can sometimes occur in tandem with intercalation. We report the first electrochemical evaluation of $NiVO_3$ as an intercalation anode material for Li-ion batteries, which offers a high capacity with negligible fading without conversion mode side reactions. Binary metal oxide $NiVO_3$ fused oxide nanoparticles (Ni-FONPs) are formed via thermal reduction of Ni-doped vanadium oxide nanotubes (Ni-VONTs). The electrochemical performance of Ni-FONPs is contrasted with a composite of Fe_2O_3 and V_2O_3 (Fe-FONPs) with a similar morphology, made using a similar process form Fe-doped VONTs. Galvanostatic cycling reveals that the binary metal oxide Ni-FONPs exhibit superior electrochemical performance compared to the Fe-FONPs by avoiding segregation into two oxides that ordinarily cycle as conversion mode material. The new anode material, Ni-FONPs, demonstrates state-of-the-art specific capacity retention (78% from the 2^{nd} to the 500^{th} cycle) and significantly long cycle life (500 cycles) when cycled using a specific current of 200 mA/g in a conductive additive and binder-free formulation. Limiting the lower voltage to ~ 0.2V avoid separate oxides of Ni and V, which independently, are detrimental to

View Article Online
DOI: 10.1039/C8TA05327H

cycle life and capacity retention. Systematic analysis of differential capacity obtained from galvanostatic voltage profiles over 500 cycles offers a detailed insight into the charge storage mechanism and electrochemical behaviour for this stable $NiVO_3$ anode material.

1 Introduction

In recent years there has been an increased demand for Li-ion batteries with high capacity and long cycle due to global objectives such as the reduction of dependence on fossil fuels via the adaptation of electric vehicles and the push towards the internet of things.[1-4] Consequently, there has been revitalized interest in vanadium oxide (VO_x) based electrode materials for Li-ion batteries due to their rich chemistry, crystallinity, and varied morphologies. [5-7] This has also led to a renewed interest in optimising the electrochemical performance of VO_x nanostructures for use as both an anode and a cathode. [8-12] Due to the multivalence nature of vanadium, many of its oxides display different electrochemical properties. For example, V_2O_5 is traditionally considered a cathode material whereas V_2O_3 is typically cycled as an anode material. [13, 14] This versatility was recently demonstrated by pairing a V_2O_3 anode with a pre-lithiated V_2O_5 cathode to prepare an all vanadium oxide full Li-ion cell. [15]

Numerous vanadium oxide nanostructures have been investigated for use as electrode materials, including nanorods, nanobelts and nanowires. [16-18] Vanadium oxide nanotubes (VONTs) offer an opportunity to dope a VO_x nanostructure with metal cations to potentially enhance their electrochemical performance. [19] VONTs typically consist of scrolled layers of vanadium oxide with primary amines intercalated between the layers, and it is this layered structure that sets them apart from myriad other nanostructured morphologies of VO_x for cation intercalation. [20-22] Amine molecules act as a structure maintaining template and facilitate scrolling during the synthesis procedure. [6] Previous reports have detailed cation exchange reactions, to exchange the organic templates with metal cations such as Ca^{2+}, Na^{+} and Co^{2+}. [23, 24] Ion exchanged VONTs have typically been treated as cathode materials, however the

Published on 28 August 2018. Downloaded by University College Cork on 9/6/2018 9:15:37 AM.

Journal of Materials Chemistry A Accepted Manuscript

View Article Online
DOI: 10.1039/C8TA05327H

Published on 28 August 2018. Downloaded by University College Cork on 9/6/2018 9:15:37 AM.

Journal of Materials Chemistry A Accepted Manuscript

modification has not halted the severe capacity fading issues associated with VONTs. For example Zhou et al. previously report on the performance of Fe-VONTs as a cathode material for Li-ion batteries. [25] It was shown that the ion exchanged VONTs offered higher capacities than the as-prepared VONTs but the ion-exchange reaction failed to mitigate significant capacity fading even after 50 cycles. Similarly Kim et al. reported on the electrochemical performance of Ni-VONTs as a cathode for Na-ion batteries and demonstrated that the capacity of the Ni-VONTs severely faded after 35 cycles. [26] We have previously reported on the structural conversion from as-prepared VONTs to V_2O_3 polycrystalline nanorods via thermal reduction in an inert atmosphere in order to address capacity fading arising from material morphology. [27-29] A similar thermal treatment of metal cation-doped VONTs opens up the possibility of preparing binary metal oxide nanostructures with crystal structures and compositions to improve electrochemical performance and stability. For oxides, especially as anodes, it is important to engineer the material not only to improve kinetics of reversible lithiation efficiency, and to avoid capacity and voltage fading, and side reactions, from conversion modes processes that can occur in tandem with intercalation.

Previous reports on metal vanadate anodes such as $Li_{1+x}V_{1-x}O_2$, $Co_3V_2O_8$, $Ni_3V_2O_8$, and MnV_2O_6 have shown that vanadium containing binary metal oxides can offer improved specific capacity and capacity retention compared to unary vanadium oxides.[30-34] For example Yang et al. reported a specific capacity of ~ 1100 mA/g after 100 cycles for $Co_3V_2O_8$ multi-layered nanosheets cycled in a potential widow of 2.5 – 0.01 V with an applied specific current of 1 A g^{-1}.[35] Charging to this low potential resulted in the conversion of $Co_3V_2O_8$ to an amorphous $Li_xV_2O_5$ matrix and the formation of CoO, which further reduced to Co and alloyed with Li.

In this report, we detail the preparation of fused oxide nanoparticles (FONPs) via thermal reduction of ion exchanged vanadium oxide nanotubes (VONTs). Initially, ion exchange reactions were performed with as-prepared VONTs and salts of the respective metals

View Article Online
DOI: 10.1039/C8TA05327H

Published on 28 August 2018. Downloaded by University College Cork on 9/6/2018 9:15:37 AM.

Journal of Materials Chemistry A Accepted Manuscript

investigated (Ni and Fe) to form Ni-VONTs and Fe-VONTs. FONPs were then prepared by annealing the ion exchanged VONTs at 700 °C in H_2/Ar. X-ray diffraction (XRD) and electron diffraction (ED) confirms that thermal treatment of Ni-VONTs resulted in the formation of a binary metal oxide in the form of $NiVO_3$ whereas thermal reduction of the Fe-VONTs produced a composite of Fe_2O_3 and V_2O_3. To our knowledge, this is the first detailed report on the structural characterisation of $NiVO_3$ and also the first report on the electrochemical properties of the compound. The electrochemical performance of Ni-FONPs and Fe-FONPs evaluated via cyclic voltammetry and long cycle life galvanostatic tests. Ni-FONPs exhibit superior electrochemical performance compared to Fe-FONPs in terms of capacity values and capacity retention. Ni-FONPs demonstrated a reversible capacity of 175 mAh/g after the 500th charge, when cycled with a specific current of 200 mA/g. This corresponded to capacity retention of 78% from the 2nd to the 500th cycle, indicating the exceptional capacity retention properties of $NiVO_3$. Through systematic analysis of differential capacity plots (DCPs) from standard galvanostatic, we present a detailed insight into how Ni-FONPs and Fe-FONPs anodes store charge and propose why the binary metal oxide outperforms the mixed composite.

2 Experimental Section

2.1 Preparation of Ion Exchanged VONTs and FONPs

VONTs were synthesized by hydrothermal treatment of a mixture of vanadium oxide xerogel and a primary amine, following previously reported procedures. [20, 21, 29] V_2O_5 xerogel was mixed with nonylamine in a molar ratio of xerogel to amine of 1:2, with 3 mL of ethanol added per gram of xerogel. The solution was mixed vigorously for 1 h and then hydrolyzed by adding 5 mL of deionized water per gram of xerogel before being mixed vigorously again for a further 2 h. The mixture was then allowed to age for 2 days. After this time the mixture turned white and was then hydrothermally treated in a Teflon lined autoclave at 180 °C for 7 days. The resulting dark black paste was washed with pure ethanol and dried using a Buchner funnel. Ion

View Article Online
DOI: 10.1039/C8TA05327H

exchanged VONTs were prepared using a modified version of a previously reported method.[19] As-synthesised VONTs were mixed with either $NiCl_2 \cdot 6H_2O$ or $FeCl_3 \cdot 6H_2O$ in a molar ratio of 1:4 to prepare Ni-VONTs or Fe-VONTs, respectively. The powders were then stirred in a solution of ethanol and water (4:1 v/v) with 0.2 ml of ethanol being added per mg of VONTs. The solutions were stirred for 5 h and then then dried on filter paper using a Buchner funnel. The ion exchanged VONTs were then heated at 700 ^oC in H_2/Ar for 6 h to prepare FONPs.

2.2 Material Characterization

Transmission electron microscopy (TEM) analysis was conducted using a JEOL JEM-2100 TEM operating at 200 kV. Scanning electron microscopy (SEM) analysis was performed using an FEI Quanta 650 FEG high resolution SEM at an accelerating voltage of 10 kV. Scanning transmission electron microscopy and EDX was carried out using a FEI Helios NanoLab 600 DualBeam FIB/SEM with an Oxford X-Max 80 EDS detector. X-ray diffraction (XRD) analysis was performed using a Phillips Xpert PW3719 diffractometer using Cu Kα radiation. (Cu Kα, λ = 0.15418 nm, operation voltage 40 kV, current 40 mA). Fourier transform infrared spectroscopy (FTIR) was conducted on Perkin Elmer Spectrum Two FT-IR Spectrometer in the region of 4000–650 cm^{-1}. X-ray photoelectron spectroscopy (XPS) spectra were acquired on an Oxford Applied Research Escabase XPS system equipped with a CLASS VM 100 mm mean radius hemispherical electron energy analyzer with multichannel detectors in an analysis chamber with a base pressure of 5.0×10^{-10} mbar. Survey scans were recorded between 0 and 1400 eV with a step size of 0.7 eV, dwell time of 0.5 s, and pass energy of 100 eV. Core level scans were acquired with a step size of 0.1 eV, dwell time of 0.5 s, and pass energy of 20 eV averaged over 10 scans. A non-monochromated Al Kα X-ray source at 200 W power was used for all scans. All spectra were acquired at a take-off angle of 90° with respect to the analyzer axis and were charge corrected with respect to the C 1s photoelectric line. Data was processed using CasaXPS software where a Shirley background correction was employed and peaks were fitted to Voigt profiles.

Published on 28 August 2018. Downloaded by University College Cork on 9/6/2018 9:15:37 AM.

Journal of Materials Chemistry A Accepted Manuscript

View Article Online
DOI: 10.1039/C8TA05327H

Published on 28 August 2018. Downloaded by University College Cork on 9/6/2018 9:15:37 AM.

Journal of Materials Chemistry A Accepted Manuscript

2.3 Electrochemical Characterization

All electrochemical results presented in this report were performed using a BioLogic VSP Potentiostat/Galvanostat. The electrochemical properties of Ni and Fe-FONP samples were investigated in a half cell configuration against a pure Li counter electrode in a two electrode, stainless steel split cell (a coin cell assembly that can be disassembled for post-mortem analysis). The electrolyte used consisted of a 1 mol dm^{-3} solution of $LiPF_6$ in a 1:1 (v/v) mixture of ethylene carbonate in dimethyl carbonate with 3 wt% vinylene carbonate. The separator used in all split cell tests was a glass fiber separator (El-Cell ECC1-01-0012-A/L, 18 mm diameter, 0.65 mm thickness). The mass loading for all FONP samples was ~ 0.5 mg, no additional conductive additives or binders were added. Cyclic voltammetry was performed using a scan rate of 0.1 mV s^{-1} in a potential window of 3.0 – 0.2 V (vs Li/Li^+). Galvanostatic cycling was performed using a range of specific currents (50 – 200 mA/g) in a potential window of 3.0 – 0.2 V (vs Li/Li^+).

3 Results and Discussion

Vanadium oxide nanotubes (VONTs) were prepared via hydrothermal treatment of a mixture of a vanadium oxide (VO_x) xerogel and nonylamine. The as-prepared VONTs consisted of three main regions; a tube opening at either end, a hollow core and layered walls on either side of the hollow core, as shown in Fig. 1a and b. We have previously reported that the interlayer spacing of the scrolled walls of the VONTs is dependent on the length of the primary amine chain, which is used during the synthesis procedure. [20] The resulting interlayer spacing for VONTs prepared with nonylamine in a molar ratio of xerogel to amine of 2:1 is ~ 2.7 nm, as shown in Fig. S1a, which agrees with our detailed quantitative measurements and analysis of the nanotube structure. [20, 21] The d-spacings observed in the electron diffraction pattern for the as-prepared VONTs are consistent with previously reported XRD patterns for VONTs. [6, 36]

View Article Online
DOI: 10.1039/C8TA05327H

Metal cation doped VONTs were prepared via facile ion exchange reactions with VONTs and salts of the respective metals investigated. [23] Nickel doped VONTs (Ni-VONTs) were prepared via an aqueous ion exchange reaction with as-prepared VONTs and $NiCl_2 \cdot 6H_2O$; iron doped VONTs (Fe-VONTs) were prepared with $FeCl_3 \cdot 6H_2O$. TEM images of typical Ni-VONTs are shown in Fig. 1d and e. It is clear that even though a quantity of the positively charged amine head group has been exchanged with Ni^+ ions the overall nanotube morphology has been retained. This is in agreement with previously reported Ni-VONTs, which were prepared via an ion exchange reaction between VONTs prepared with octadecylamine and $NiCl_2$. [26] There is a significant decrease in the interlayer spacing for the Ni-VONTs (~0.9 nm) compared to the as-prepared VONTs (~2.7 nm), as shown in Fig. S1b.

Published on 28 August 2018. Downloaded by University College Cork on 9/6/2018 9:15:37 AM.

Journal of Materials Chemistry A Accepted Manuscript

View Article Online
DOI: 10.1039/C8TA05327H

Published on 28 August 2018. Downloaded by University College Cork on 9/6/2018 9:15:37 AM.

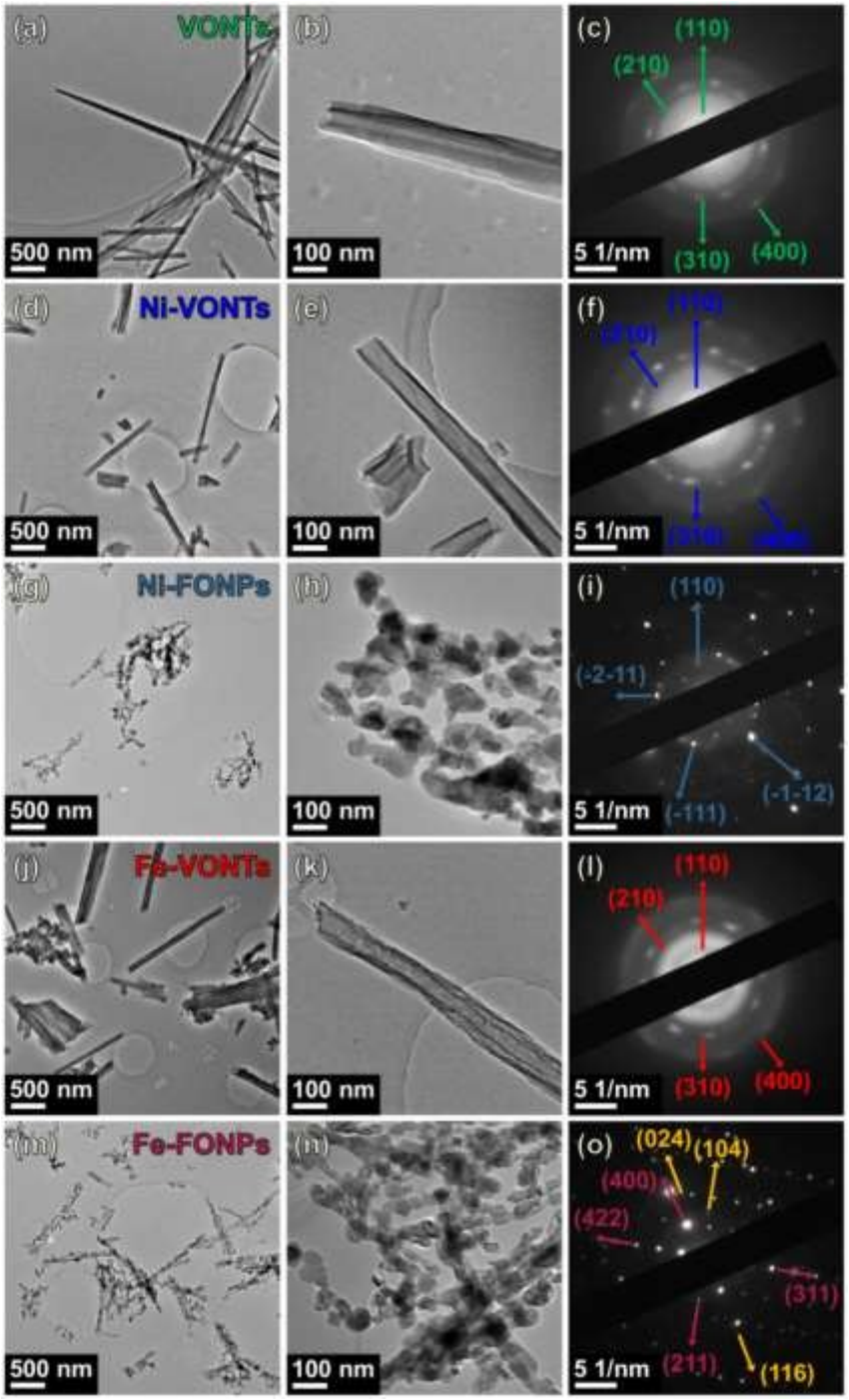


Fig. 1. (a) and (b) TEM images and (c) electron diffraction pattern for as-prepared VONTs. (d) and (e) TEM images and (f) electron diffraction pattern for Ni-VONTs. (g) and (h) TEM images and (i) electron diffraction pattern for Ni-FONPs. (j) and (k) TEM images and (l) electron diffraction pattern for Fe-VONTs. (m) and (n) TEM images and (o) electron diffraction pattern for Fe-FONPs. (• indexed to V_2O_3, JCPDS No. 00-034-0187, • indexed Fe_2O_3, JCPDS No. 00-039-1346).

Likewise, the overall nanotube morphology is also retained for the Fe-VONTs as shown in Fig. 1j and k. This is in agreement with similar Fe-VONTs which were prepared via a metal cation exchange reaction involving VONTs prepared with dodecylamine and $FeCl_3 \cdot 6H_2O$.[25]

Journal of Materials Chemistry A Accepted Manuscript

View Article Online
DOI: 10.1039/C8TA05327H

Published on 28 August 2018. Downloaded by University College Cork on 9/6/2018 9:15:37 AM.

Journal of Materials Chemistry A Accepted Manuscript

The interlayer spacing of the Fe-VONTs is ~ 1.4 nm (Fig. S1d), which is also smaller than observed for the as-prepared VONTs. The electron diffraction patterns for the Ni-VONTs and Fe-VONTs, shown in Fig. 1f and l, respectively, are in close agreement with the pattern observed for the as-prepared VONTs. This suggests that the ion exchange reactions do not significantly alter the crystal structure of the layers of vanadium oxide present within the scrolled walls of the nanotubes. Annealing Ni-VONTs and Fe-VONTs to 700 °C in H_2/Ar resulted in a structural conversion from nanotubes to fused oxide nanoparticles (FONPs). TEM images of Ni-FONPs and Fe-FONPs are shown in Fig. 1 (d and e) and (m and n), respectively. Thermal treatment to this temperature removes any amine molecules remaining after ion exchange reactions and consequently the nanotube structure collapses to enable recrystallization to beaded rods of fused nanoparticles.

The lattice spacing for the Ni-FONPs and Fe-FONPs were measured to be ~ 0.34 and 0.29 nm, respectively, as shown in Fig. S1c and e. Although the electron diffraction patterns for the Ni-VONTs and the Fe-VONTs were quite similar, the diffraction patterns for both samples after annealing are significantly different. The d-spacings in the electron diffraction for the Ni-FONPs are consistent with those previously reported for $NiVO_3$ (JCPDS No. 00-027-1308), whereas the electron diffraction for the Fe-FONPs consists of two sets of diffraction spots, one can be indexed to V_2O_3 (JCPDS No. 00-034-0187) and the other to Fe_2O_3 (JCPDS No. 00-039-1346). This implies that the Ni-FONPs are a single nickel vanadium oxide, in the form of $NiVO_3$, whereas the Fe-FONPs are a composite of two different compounds, V_2O_3 and Fe_2O_3. The chemical composition of the FONP samples will be further probed via XRD and XPS analysis. A schematic representation of the eventual structural conversion from as-prepared VONTs to FONPs is shown in Fig. 2a. The tubular morphology of the as-prepared VONTs is preserved after the ion exchange reactions; the hollow core of both the Ni-VONTs and Fe-VONTs is wider than for the as-prepared VONTs. Thermal reduction in H_2/Ar results

in a significant structural conversion from nanotubes to beaded rods of fused oxide nanoparticles.

View Article Online
DOI: 10.1039/C8TA05327H

The XRD pattern observed for the as-prepared VONTs is in close agreement with previously reported XRD patterns for VONTs prepared with amines of various chain lengths. [37-39] The XRD patterns for the Ni-VONTs and Fe-VONTs are quite similar to the pattern observed for the as-prepared VONTs, as shown in Fig. 2b and c. Within the layered walls of the as-prepared VONTs the positively charged NH^{3+} amine head group is electrostatically bound to a negatively charged O^-, during the ion exchange reaction the NH^{3+} head group is exchanged with metal cations, and afterwards the metal cations are electrostatically bound to the O^-. [20, 25, 40] The ion exchange reaction does not significantly alter the crystal structure of the host nanotube and consequently the XRD patterns for Ni-VONTs and Fe-VONTs are a close match with the pattern observed for the as-prepared VONTs. We have previously reported that the XRD pattern for ion exchanged Na-VONTs was also a close match with as-prepared VONTs [19] and a similar observation was also made for Mn-VONTs. [41] The intensity of some of the initially lower intensity reflections such as (110) and (200) reduced after the initial metal ion exchange, a similar phenomenon was previously reported for Fe-VONTs.[25] This effect arises from a puckering or buckling of the typically ordered lamellar structure of the VONTs while accommodating intercalated cations or organic moieties[20, 22]. Low index reflections stem from the crystal structure of molecularly thick layers in orthorhombic V_2O_5, which are periodically spaced and ordered in VONTs, but become buckled after cation intercalation, but remain crystalline.

There are significant differences in the XRD patterns observed for the heat-treated FONPs, compared to the VONTs. XRD analysis confirmed the ion exchange and recrystallization process from VONTs to FONPs, resulted in a fused nanoparticle structure of high aspect ratio, similar to a granular nanowire. The pattern for Ni-FONPs demonstrated high intensity reflections associated with $NiVO_3$. There is very little information about the structural

Published on 28 August 2018. Downloaded by University College Cork on 9/6/2018 9:15:37 AM.

Journal of Materials Chemistry A Accepted Manuscript

View Article Online
DOI: 10.1039/C8TA05327H

Published on 28 August 2018. Downloaded by University College Cork on 9/6/2018 9:15:37 AM.

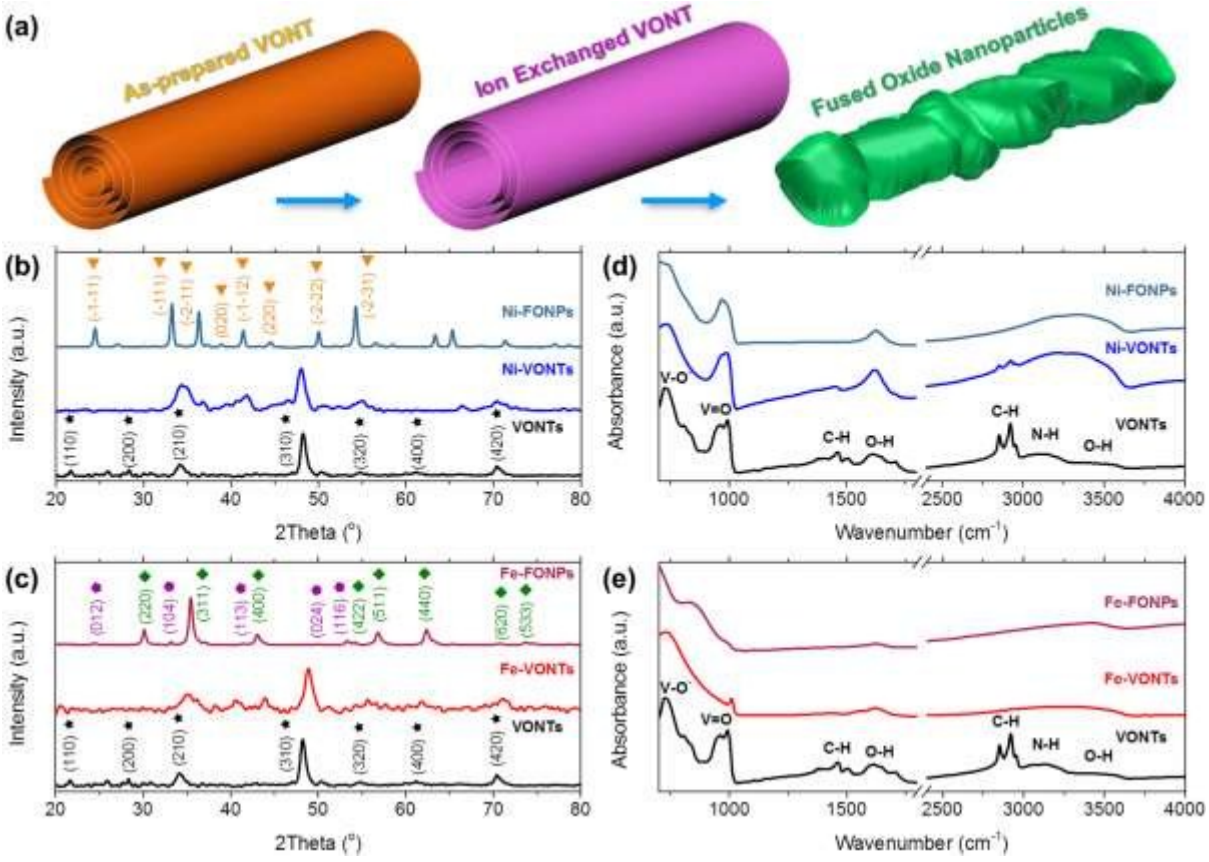
properties of $NiVO_3$ in the literature. To our knowledge, there is only one paper detailing the structural characteristics of this material. Chamberland presented the reference pattern for $NiVO_3$ (JCPDS No. 00-027-1308) in 1970. [42] The XRD pattern that we observe for our Ni-FONPs is a very close match, and corroborated by detailed compositional and surface chemistry characterization in our work. The XRD pattern observed for Ni-FONPs is also a close match with a previously reported pattern for $CoVO_3$, as shown in Fig. S2, which has a similar triclinic crystal system, and $CuVO_3$ is also a related phase.[43] None of the other nickel vanadates, such as $Ni_3V_2O_8$ as a notable anode material, show similar diffraction patterns. The XRD pattern for the Fe-FONPs consists of peaks associated with Fe_2O_3 and V_2O_3, implying that Fe-FONPs are a composite of both materials. We have previously reported that when VONTs are heated to 600 ^oC in N_2, V_2O_3 polycrystalline nanorods (poly-NRs) are formed. [27, 28, 44] Indexing of the XRD patterns for heated ion exchanged VONTs indicates that annealing the Ni-VONTs resulted in the formation of a binary metal oxide in the form of $NiVO_3$. Annealing the Fe-VONTs did not result in the formation of an Fe-V oxide, instead a composite of Fe_2O_3 and V_2O_3 was formed. Ni-VONTs and Fe-VONTs are metal-doped VONTs however after thermal treatment, NI-FONPs are a binary oxide and Fe-VONTs are a composite of two distinct oxides. The chemical composition of the ion exchanged VONTs and FONPs will be discussed in further detail during the EDS and XPS analysis. Structurally, the use of a starting VONT nanotube structure allow an ion exchange and recrystallization process using different cations to form separate single and dual phase products, while retaining the dominant fused nanoparticle morphology for all materials. SEM images of the ion exchanged VONTs and heat treated FONPs are and corresponding energy-dispersive X-ray spectroscopy (EDS) spectra are shown in Fig. S3 and spatial mapping in Fig. S4. The EDS spectra for VONT and FONP samples contained peaks associated with V and O and the ion exchanged metal (either Ni or Fe). We observed a similar trend for both Ni-VONTs and Fe-VONTs after thermal treatment in H_2/Ar; the relative amounts of O decreased for both samples decreased and the relative

Journal of Materials Chemistry A Accepted Manuscript

View Article Online
DOI: 10.1039/C8TA05327H

amounts of Ni and Fe increased respectively. A peak associated with the presence of Cl, from the metal precursors, was observed in the spectra for the VONT samples but was no longer present after thermal treatment for the FONP samples.

FTIR spectra were acquired for the VONT and FONP materials to confirm that the ion exchange reaction between the positively charged amine head groups and metal cations was successful. The peaks observed between 1460-1650 cm^{-1} and 2850-2930 cm^{-1} are attributed to C-H bending and stretching vibrations respectively and are due to the presence of amine molecules. [22, 45, 46] The intensity of these peaks significantly decreased for both the Ni-VONTs and Fe-VONTs, as shown in Fig. 2d and e, confirming that the ion exchange between the amino groups and the intercalated cations did occur. Upon heating to 700 °C in H_2/Ar, the vibration mode intensity associated with the amine molecules were no longer present. The data suggests that annealing to this temperature removed all measurable presence of amines between the layers of vanadium oxide.



Published on 28 August 2018. Downloaded by University College Cork on 9/6/2018 9:15:37 AM.

Journal of Materials Chemistry A Accepted Manuscript

View Article Online
DOI: 10.1039/C8TA05327H

Fig. 2. (a) Schematic representation of the structural conversion from as-prepared VONTs to ion exchanged VONTs via a metal cation exchange reaction and then to fused oxide nanoparticles via annealing to 700 °C in H_2/Ar. XRD patterns for (b) Ni-VONTs and Ni-FONPs and (c) Fe-VONTs and Fe-FONPs. (▼ = $NiVO_3$, JCPDS No. 00-027-1308, ◆ = V_2O_3, JCPDS No. 00-034-0187, ● = Fe_2O_3, JCPDS No. 00-039-1346). FTIR spectra for (d) Ni-VONTs and Ni-FONPs and (e) Fe-VONTs and Fe-FONPs.

X-ray photoelectron spectroscopy (XPS) spectra were acquired for each material to determine the surface chemical state of single phase $NiVO_3$ and the nature of the binary Fe_2O_3 and V_2O_3 composite FONPs. Two main peaks can be seen in the Ni 2p spectrum for the Ni-VONTs at ~ 855.9 and 873.9 eV, corresponding to the Ni $2p_{3/2}$ and $2p_{1/2}$ levels respectively. [47] Both of these peaks contain shoulders and can be deconvoluted, indicating that they are composed of a mixture of Ni^{2+} and Ni^{3+}, as shown in Fig. 3a. Core-level emission associated with Ni^{2+} and Ni^{3+} are located at ~ 855.8 and 856.5 eV, respectively. [48] Two satellite peaks are also observed at ~ 862.3 and 880.3 eV. Comparison of the integrated areas of the peaks associated with each valence state indicates that the majority (~ 72%) of Ni present within the Ni-VONTs was in the Ni^{3+} valence state. However, after the structural conversion from Ni-VONTs to Ni-FONPs the majority of Ni is in the Ni^{2+} valence state (~ 66%). XPS spectra demonstrating the core level binding energies for V $2p_{3/2}$ and V $2p_{1/2}$ for Ni-VONTs and Ni-FONPs are shown in Fig. 3c and d, respectively. Both samples contain V in the V^{5+} and V^{4+} oxidation states with no difference in the relative amounts of each after thermal treatment, as listed in Table S2. Considering that the majority of the Ni present within the Ni-FONPs is in the Ni^{2+} oxidation state and the majority of the V is in the V^{4+} state, XPS analysis is in close agreement with the XRD pattern for the Ni-FONPs which suggests that they are predominantly composed of $NiVO_3$.

The Fe 2p region for the Fe-VONTs shows two main peaks at ~710.0 and 724.8 eV corresponding to the Fe $2p_{3/2}$ and Fe $2p_{1/2}$ core levels, respectively, and two satellite peaks at 719.2 and 733.2 eV. [49, 50] The Fe 2p spectrum was fitted to two spin–orbit doublets characteristic of Fe^{2+} and Fe^{3+}, as shown in Fig. 3e, which indicates that Fe within the Fe-

Published on 28 August 2018. Downloaded by University College Cork on 9/6/2018 9:15:37 AM.

Journal of Materials Chemistry A Accepted Manuscript

View Article Online
DOI: 10.1039/C8TA05327H

VONTs is present in both oxidation states. The Fe $2p_{3/2}$ and Fe $2p_{1/2}$ core levels for the Fe-FONPs are shifted to slightly higher energies that the Fe-VONTs, having peaks at ~ 711.2 and 725.0 eV, respectively. Similar to the Fe-VONTs, the Fe 2p spectrum for the Fe-FONPs could be deconvoluted to demonstrate contributions from both Fe^{2+} and Fe^{3+}, as shown in Fig. 3f. The relative amounts of Fe present in both oxidation states for Fe-VONTs and Fe-FONPs are listed in Table S2. Comparison of the integrated areas of the peaks associated with each valence state indicates that ~ 37% of Fe present in the Fe-VONTs was in the Fe^{3+} valence state, after annealing the amount of Fe^{3+} present in the Fe-FONPs remained close to this value (~ 35%).

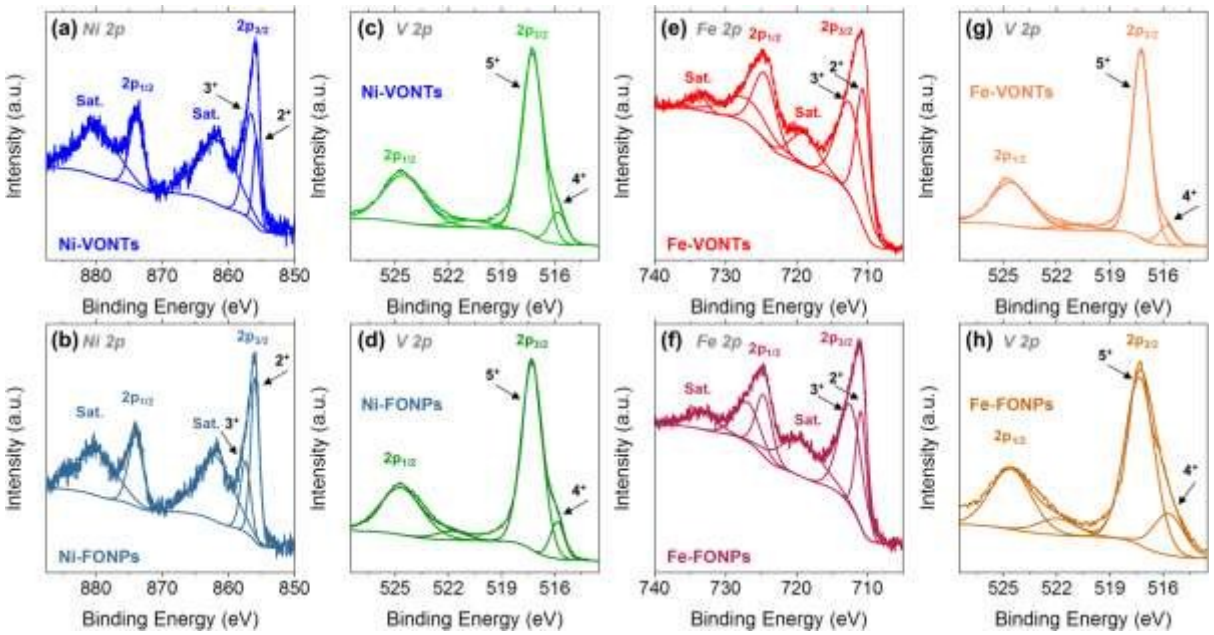


Fig. 3. XPS spectra of the Ni 2p regions for (a) Ni-VONTs and (b) Ni-FONPs, V 2p regions for (c) Ni-VONTs and (d) Ni-FONPs, Fe 2p regions for (e) Fe-VONTs and (f) Fe-FONPs and the V 2p regions for (g) Fe-VONTs and (h) Fe-FONPs.

XPS spectra showing the core level binding energies for V $2p_{3/2}$ and V $2p_{1/2}$ acquired for Fe-VONTs and Fe-FONPs are shown in Fig. 3g and h, respectively. The V 2p core-levels for both samples can be deconvoluted to demonstrate the contributions of vanadium present in different oxidation states. The V $2p_{3/2}$ core-level for Fe-VONTs and Fe-FONPs consisted of two deconvoluted peaks at ~517.2 and 515.8 eV, which correspond to the presence of V^{5+} and

Published on 28 August 2018. Downloaded by University College Cork on 9/6/2018 9:15:37 AM.

Journal of Materials Chemistry A Accepted Manuscript

View Article Online
DOI: 10.1039/C8TA05327H

V^{4+}, respectively. [51, 52] Initially ~ 91% of the V present in the Fe-VONTs was in the V^{5+} oxidation state, after thermal treatment in Ar, this decreased to ~ 80%, indicating that V, present within the Fe-VONTs, has been partially reduced. The reduction of V_2O_5 via annealing under an inert atmosphere has been previously reported for V_2O_5 gels and nanocrystals. [53, 54] XPS spectra of the O 1s regions for Ni-VONTs, Ni-FONPs, Fe-VONTs and Fe-FONPs are shown in Fig. S5.

Cyclic voltammetry was performed to compare the electrochemical response of the binary metal oxide Ni-FONPs and the Fe_2O_3/V_2O_3 composite Fe-FONPs. To our knowledge this report represents the first electrochemical investigation of $NiVO_3$ as an intercalation electrode material for Li-ion batteries, consequently the redox behaviour of $NiVO_3$ has not yet been established. A reduction peak was observed at ~ 1.04 V during the initial cathodic scan which is at the same potential as the peak seen during the first scan for the Fe-FONPs, and may be attributed to the formation of an SEI layer. [55, 56] We propose that the reduction peak at ~ 0.56 V is due to the lithiation of $NiVO_3$ as follows:

$$NiVO_3 + xLi^+ + xe^- \leftrightarrow Li_xNiVO_3 \qquad \text{Eqn. 1}$$

The potential of this peak does not significantly change over 10 CV scans, indicating that this intercalation process is highly reversible, however it is clear from the current values in Fig. 4a that there is an increase in the charge stored due to this process over the initial 10 cycles. It can be seen in Fig. 4a that the charge stored due to the intercalation process decreased after the 2nd and 5th cycles but increased after the 10th cycle. The increased charge stored may be due to additional intercalation sites becoming exposed as a result of the initial few cycles; this will be discussed in greater detail during the analysis of the capacity values obtained from galvanostatic cycling. We propose that the oxidation peak at ~ 1.15 V during the initial anodic scan is due to the delithiation of Li_xNiVO_3. The charge stored due to the delithiation process also increased after the 10th cycle.

Published on 28 August 2018. Downloaded by University College Cork on 9/6/2018 9:15:37 AM.

Journal of Materials Chemistry A Accepted Manuscript

View Article Online
DOI: 10.1039/C8TA05327H

A series of reduction peaks were observed in the initial cathodic scan for the Fe-FONPs as shown in Fig. 4b. The peak at ~ 1.04 V is due to the formation of the SEI layer [57, 58] and is not observed in subsequent cycles. The peak at 0.68 V can be attributed to the intercalation of Li^+ into the V_2O_3 component of the Fe-FONPs as follows [59, 60]:

$$V_2O_3 + xLi^+ + xe^- \leftrightarrow Li_xV_2O_3 \qquad \text{Eqn. 2}$$

The peak at ~ 0.22 V may be ascribed to the reduction of $Li_xV_2O_3$ and the formation of Li_2O as follows:

$$Li_xV_2O_3 + (6 - x)Li^+ + (6 - x)e^- \leftrightarrow 2V + 3Li_2O \qquad \text{Eqn. 3}$$

The relatively weak peak at ~ 0.38V is likely due to the reduction of the Fe_2O_3 component of the Fe-FONPs as follows [61]:

$$Fe_2O_3 + 6Li^+ + 6e^- \leftrightarrow 2Fe + 3Li_2O \qquad \text{Eqn. 4}$$

Two strong oxidation peaks were observed in the first anodic scan for the Fe-FONPs at ~ 1.20 and 2.10 V. The potentials of these peaks are in close agreement with previously reported values for V_2O_3 based anode materials and correspond to the multistep oxidation of V^{2+} and V^{3+} to higher valance states. [14, 15] It is clear from the first CV scan that the V_2O_3 component of the Fe-FONPs dominates the charge storage process, and relatively weak intensity peaks associated with the Fe_2O_3 component are observed. There are significant differences in the CV response of the Ni-FONPs compared to the Fe-FONPs. One key contributing factor to this difference is that, according to the XRD patterns acquired for both samples, the Fe-FONPs are a composite of Fe_2O_3 and V_2O_3, whereas the Ni-FONPs are primarily a single phase, binary metal oxide in the form of $NiVO_3$.

Published on 28 August 2018. Downloaded by University College Cork on 9/6/2018 9:15:37 AM.

Journal of Materials Chemistry A Accepted Manuscript

View Article Online
DOI: 10.1039/C8TA05327H

Published on 28 August 2018. Downloaded by University College Cork on 9/6/2018 9:15:37 AM.

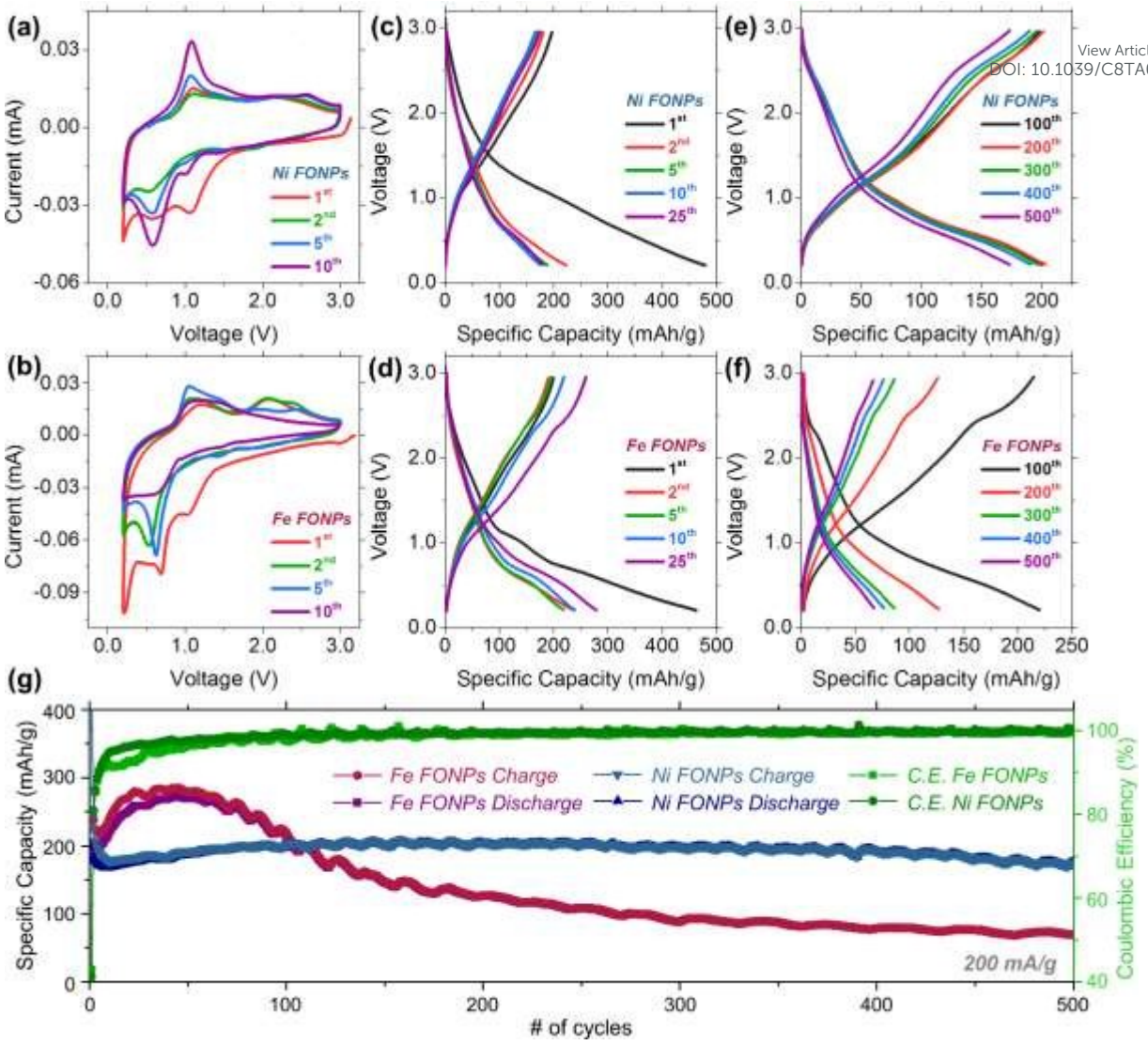


Fig. 4. Cyclic voltammograms showing the 1st, 2nd, 5th and 10th cycles, for (a) Ni-FONPs and (b) Fe-FONPs, cycled in a potential window from 3.0 – 0.01 V at a scan rate of 0.1 mV/s. Charge and discharge voltage profiles for the 1st, 2nd, 5th, 10th and 25th cycles for (c) Ni-FONPs and (d) Fe-FONPs and for the 100th, 200th, 300th, 400th and 500th cycles for (e) Ni-FONPs and (f) Fe-FONPs at a specific current of 200 mA/g in a potential window of 3.0 – 0.01 V (vs Li/Li^+). (g) Comparison of the specific capacity values and coulombic efficiency obtained for Ni-FONPs and Fe-FONPs over 500 cycles.

The electrochemical performance of the FONPs was further investigated via galvanostatic cycling. FONP samples were charged and discharged for 500 cycles using a specific current of 200 mA g^{-1}. A selection of the resulting charge and discharge curves obtained over 500 cycles for Ni-FONPs and Fe-FONPs are presented in Fig. 4. The voltage profiles for the 1st charge and discharge for Ni-FONPs are shown in Fig. 4c. The initial charge and discharge capacities were ~479 and 197 mAh/g, respectively, corresponding to an initial

Journal of Materials Chemistry A Accepted Manuscript

View Article Online
DOI: 10.1039/C8TA05327H

Published on 28 August 2018. Downloaded by University College Cork on 9/6/2018 9:15:37 AM.

Journal of Materials Chemistry A Accepted Manuscript

Coulombic efficiency (ICE) of ~ 41%. The large initial capacity may be attributed to defects induced in the crystal structure of the Ni-FONPs due to thermal annealing at 700 °C as well as formation of an SEI layer on the surface of the material. [62] The stability of the $NiVO_3$ material as an anode down to a lower potential limit of 0.2 V (vide infra) is demonstrated by the repeatable voltage profile over 500 cycles. From 2nd to 500th cycle, the material in a binder and conductive additive-free formulation exhibits a voltage fade of ~290 mV compared to ~600 mV for Fe-FONPs. Voltages were extracted at just 50 mAh g^{-1} capacity so that a comparison value can be extracted from the unstable Fe-FONPs material, and represents the regions where the largest voltage changes occur for these materials.

Differential capacity plots (DCPs) were determined from the 1st charge and discharge curves for Ni-FONPs and Fe-FONPs, as shown in Fig. S6. Two distinct peaks were observed in the DCP of the 1st charge for the Ni-FONPs as shown in Fig. S6a. The peak centred at ~ 1.1 V is most likely due to the formation of an SEI layer and the peak at ~ 0.6 V may be attributed to the lithiation of $NiVO_3$ as in Eqn. 1. The potential of both of these peaks are in close agreement with observations from the first CV scan shown in Fig. 4a. The profiles of the charge and discharge curves for the Ni-FONPs do not significantly change from the 2nd to the 500th cycle, demonstrating the highly reversible the lithiation/delithiation of $NiVO_3$ even in a formulation free of any binder or conductive additive. The capacity values obtained for the Ni-FONPs over hundreds of cycles are quite stable from the 2nd cycle onwards, which again is indicative of a highly reversible process.

The initial charge and discharge capacities for the Fe-FONPs were ~463 and 200 mAh/g, respectively, corresponding to an initial Coulombic efficiency (ICE) of ~ 43%, slightly higher than the ICE observed for the Ni-FONPs (41%). The 1st charge curve for Fe-FONPs consisted of three regions. The sloping region from 3.0 - 1.1 V can be attributed to the formation of an SEI layer. [57, 58] The regions from 1.1 – 0.8 V and from 0.8 – 0.2 V correspond to the lithiation of the V_2O_3 component of the Fe-FONPs and the reduction of the Fe_2O_3 component

View Article Online
DOI: 10.1039/C8TA05327H

Published on 28 August 2018. Downloaded by University College Cork on 9/6/2018 9:15:37 AM.

Journal of Materials Chemistry A Accepted Manuscript

of the Fe-FONPs, respectively. [63, 64] These distinct sloping regions can be clearly identified as peaks in the DCP of the 1st charge curve for Fe-FONPs, shown in Fig. S6a. The specific capacity values for the Fe-FONPs increased over the initial 50 cycles before gradually fading over the remainder of the 500 cycles. The initial increase in capacity may be attributed to a number of factors such as additional charge storage sites becoming available during initial cycles as a result of the reduction of the V_2O_3 and Fe_2O_3 components of the Fe-FONPs as well as the activation process with the lithium-ion diffusion path gradually being established in the electrode material. [65-67] For the conversion-mode contributions, Li_2O formation also adds to cumulative charge, and the reduced efficiency for coulombically balanced decomposition and reformation per cycle becomes apparent after 50 cycles in the V_2O_3-Fe_2O_3 composite. Such initial cycle instability is not found for lithiation of $NiVO_3$ as Ni-FONPs.

A comparison of the specific capacity values obtained for Ni-FONPs and Fe-FONPs cycled with a specific current of 200 mA/g for 500 cycles, and their related Coulombic efficiencies are shown in Fig. 4g. The Ni-FONPs offered superior capacity retention with much more stable capacity retention compared to the Fe-FONPs over hundreds of cycles, at a high rate. The charge capacity for the Ni-FONPs after the 2nd cycle was 225 mAh/g, and there was little variation in the charge capacities from the 2nd cycle onwards. Ni-FONPs achieved a reversible capacity of ~ 203 and 175 mAh/g after the 250th and 500th cycles respectively, corresponding to capacity retention of ~ 90% and 78% from the 2nd cycle. The average charge capacity for Ni-FONPs from the 2nd to the 500th cycle was 195 mAh/g. This high level of capacity retention over hundreds of cycles at a fast rate demonstrates the efficient reversibility of the lithiation/delithiation of $NiVO_3$. The excellent capacity retention of the Ni-FONPs is also clear from the Coulombic efficiency. After the first 10 cycles the Coulombic efficiency was > 95% for the remainder of the 500 cycles. The capacity values for the Fe-FONPs increased significantly over the initial ~ 50 cycles before fading gradually over the remainder of the 500 cycles. This gradual fading is common with conversion mode anode materials, we have

View Article Online
DOI: 10.1039/C8TA05327H

previously reported similar trends for Co_3O_4 and other mixed transition metal oxides.[68-71] Fe-FONPs gave charge capacities of ~ 110 and 70 mAh/g after the 250th and 500th cycles respectively, corresponding to capacity retentions of ~ 46 and 29% from the 2nd cycle. The enhanced capacity stability of the single phase Ni-FONPs compared to the composite Fe-FONPs is evident from long cycle life testing.

Our FONP samples were cycled in a potential window of 3.0 – 0.2 V (vs. Li/Li^+). Other previously reported vanadium containing binary metal oxide anodes such as $Ni_3V_2O_8$ and $Co_3V_2O_8$ were typically cycled to a lower potential limit of 0.01 V (vs. Li/Li^+).[72, 73] It has been suggested for these materials that during the first charge $M_3V_2O_8$ (M = Ni or Co) is reduced to form MO and an amorphous $Li_xV_2O_8$ matrix. The unary metal oxide may also alloy with Li to form Li_xM. We determined that cycling our FONP samples to the lower limit of 0.01 V had a detrimental effect of their electrochemical performance, as shown in Fig. S7. The initial capacities for both the Ni-FONPs and Fe-FONPs were higher when charged down to 0.01 V (vs. Li/Li^+) compared to FONP samples charged to 0.2 V, however both samples suffered from severe capacity fading after ~ 25 cycles. It is evident from Fig. S7 that FONP samples, in particular Ni-FONPs, demonstrated enhanced capacity retention when charged to the 0.2 V compared to samples cycled to the lower potential of 0.01 V, avoiding formation of MO phases.

We propose the superior performance of the Ni-FONPs compared to the Fe-FONPs is due to the Ni-FONPs being an intercalation-mode binary metal oxide in the form of $NiVO_3$, compared to the Fe-FONPs as a composite of Fe_2O_3 and V_2O_3. Fe_2O_3 and NiO behave as conversion mode materials with intrinsic capacity fading issues and cycle-related side reactions. [74, 75] $NiVO_3$ behaves as an intercalation mode material and consequently cycles with significantly increased stability compared to the Fe_2O_3-based composite Fe-FONPs. To interrogate the behaviour of the materials after cycling, we analysed SEM images of Ni and Fe-FONP samples before and after 500 galvanostatic cycles are shown in Fig. S8. While Ni and Fe-FONP materials crystallize to a similar morphology, but with markedly different

Published on 28 August 2018. Downloaded by University College Cork on 9/6/2018 9:15:37 AM.

Journal of Materials Chemistry A Accepted Manuscript

View Article Online
DOI: 10.1039/C8TA05327H

crystalline composition as identified by XRD, both materials look significantly different after 500 cycles. Ni-FONPs in the $NiVO_3$ acts as an intercalation mode material, and consequently we observe some swelling of the beaded nanorods such that the coulombically stable long term cycled morphology is that of larger interconnected particles. Conversely, the Fe-FONPs are a composite of Fe_2O_3 and V_2O_3 and behave as a conversion mode material. As a result, the beaded structure is completely destroyed after 500 cycles and this pulverisation may also contribute towards the lower capacity values which were observed for the Ni-FONPs compared to the Fe-FONPs. We also find characteristic evidence of Li_2O formation from conversion mode processes on the surface of the Fe-FONPs material following Eqns 3 and 4 that incurs a reversible charge penalty during cycling as demonstrated here, and this additional material is completely absent in the intercalation mode Ni-FONPs. EDS spectra for Ni and Fe-FONP samples after 500 cycles are shown in Figs S3 and discussed in the SI.

Published on 28 August 2018. Downloaded by University College Cork on 9/6/2018 9:15:37 AM.

Journal of Materials Chemistry A Accepted Manuscript

View Article Online
DOI: 10.1039/C8TA05327H

Published on 28 August 2018. Downloaded by University College Cork on 9/6/2018 9:15:37 AM.

Journal of Materials Chemistry A Accepted Manuscript

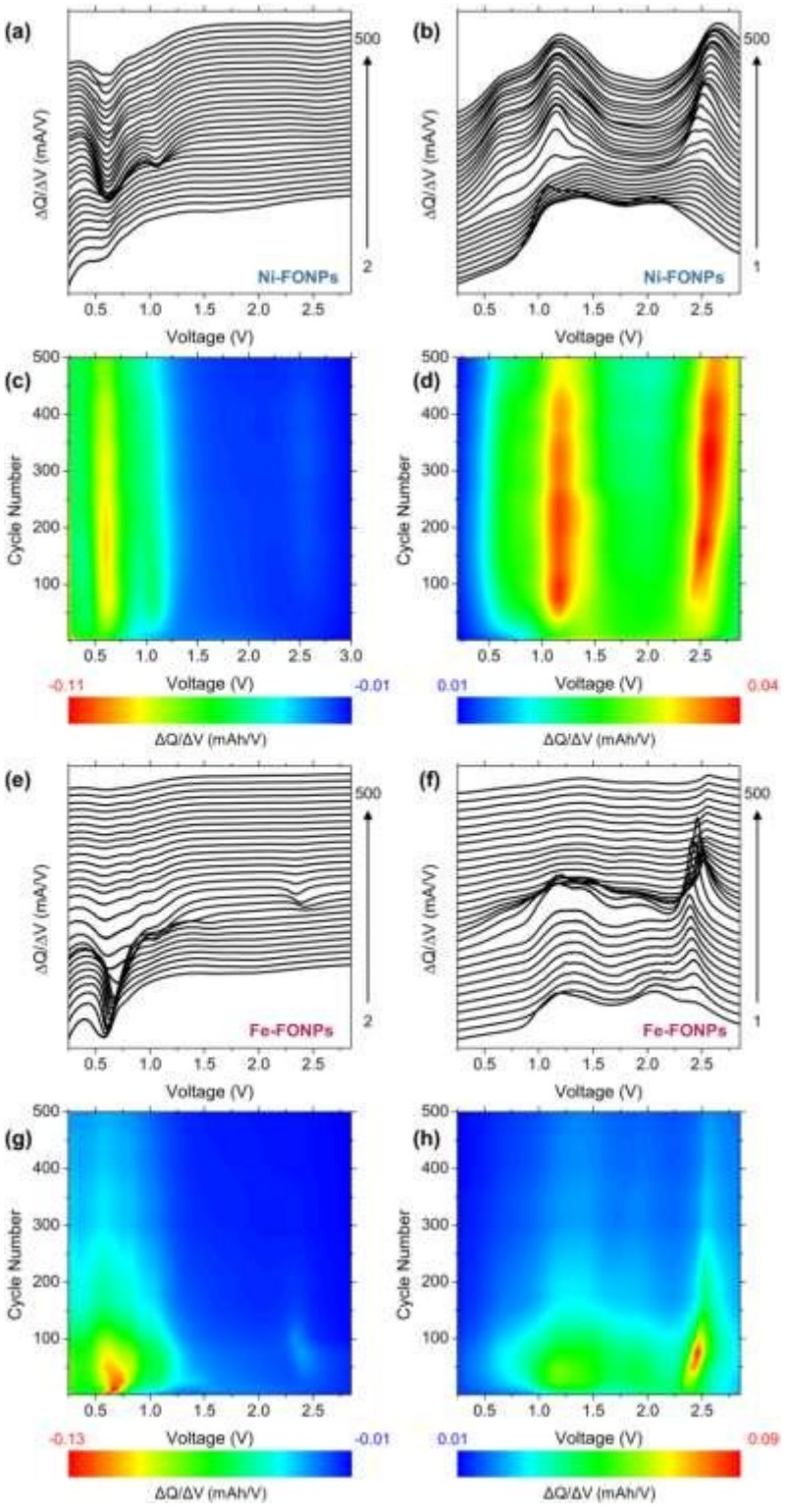


Fig. 5. Differential capacity plots calculated from (a) the charge curves and (b) the discharge curves for Ni-FONPs cycled at 200 mA/g and (c) and (d) the respective differential capacity colour maps. Differential capacity plots calculated from (e) the charge curves and (f) the discharge curves for Fe-FONPs cycled at 200 mA/g and (g) and (h) the respective differential capacity colour maps. Differential capacity plots are shown for a range of charges/discharges from the 2nd to the 250th charge (every 25th curve shown after the first 10 charges).

View Article Online
DOI: 10.1039/C8TA05327H

Published on 28 August 2018. Downloaded by University College Cork on 9/6/2018 9:15:37 AM.

DCPs, shown in Fig. 5, were calculated for a series of charge and discharge curves from the 1st to the 500th cycle to investigate the potential dependent charge storage mechanism. The DCPs of the charge curves for Ni-FONPs consistently exhibited a reduction peak at ~ 0.60 V from the 1st to the 500th cycle. This peak is associated with the lithiation of $NiVO_3$ and its presence in all 500 cycles confirms that the lithiation of $NiVO_3$ is a highly reversible process. The DCPs of the discharge curves Ni-FONPs consisted of two strong peaks centred at ~1.2 and 2.5 V, corresponding to the multistep delithiation of Li_xNiVO_3. A similar oxidation peak at ~2.5 V was reported for VO_x/C nanoscroll anodes. [76] The consistency of the potentials at which these peaks occur over 500 cycles is further evidence of the highly reversible delithiation of Li_xNiVO_3. Notably, the material exhibits negligible voltage fade for the primary reversible charge storage processes. The DCPs of the charge curves for the Fe-FONPs demonstrate that the lithiation of V_2O_3 as explained by Eqn. 2 dominates the charge storage mechanism for approximately the first 100 cycles, as can be seen by the high intensity reduction peak at ~ 0.68 V in the colour map in Fig. 5g. However, from the DCPs in Fig. 5e and the corresponding colour map in Fig. 5e, the intensity of this reduction peak gradually decreases from the 100th to the 500th cycle. The gradual cessation of the reduction process occurring at this potential is responsible for the capacity fading observed for Fe-FONPs, shown in Fig. 4g. Likewise the oxidation peaks observed at ~ 1.2 and 2.3 V, due the multistep oxidation of V^{2+} and V^{3+} to higher valance states, also fade significantly after the initial 100 cycles.

As the binary metal oxide $NiVO_3$ FONPs demonstrated significantly higher capacities as well as superior capacity retention compared to the mixed composite Fe_2O_3/V_2O_3 FONPs, the galvanostatic response of the Ni-FONPs was further investigated via cycling at a slower rate. A selection of the resulting charge and discharge curves over 100 cycles using a specific current of 50 mA/g are shown in Fig. 7a and b. The voltage profiles are similar to those shown in Fig. 4b and c, but the specific capacity is considerably higher. The initial charge and discharge capacities were ~ 2255 and 885 mAh/g, respectively corresponding to an ICE of 39%

Journal of Materials Chemistry A Accepted Manuscript

View Article Online
DOI: 10.1039/C8TA05327H

which is similar to the ICE of ~ 41% observed when using a higher specific current of 200 mA/g. The Ni-FONPs demonstrated a large reversible capacity of ~ 420 mAh/g after 100 cycles. Compared to the specific capacity obtained when cycled at 200 mA/g (Fig. 4g), the capacity after 100 cycles increased by a factor of 2 when the applied specific current was reduced by a factor of 4. The impressive capacity retention of the Ni-VONTs is also evident in the Coulombic efficiency values observed, after 15 cycles the Coulombic efficiency was > 95% and remained above this value for the remainder of the 100 cycles.

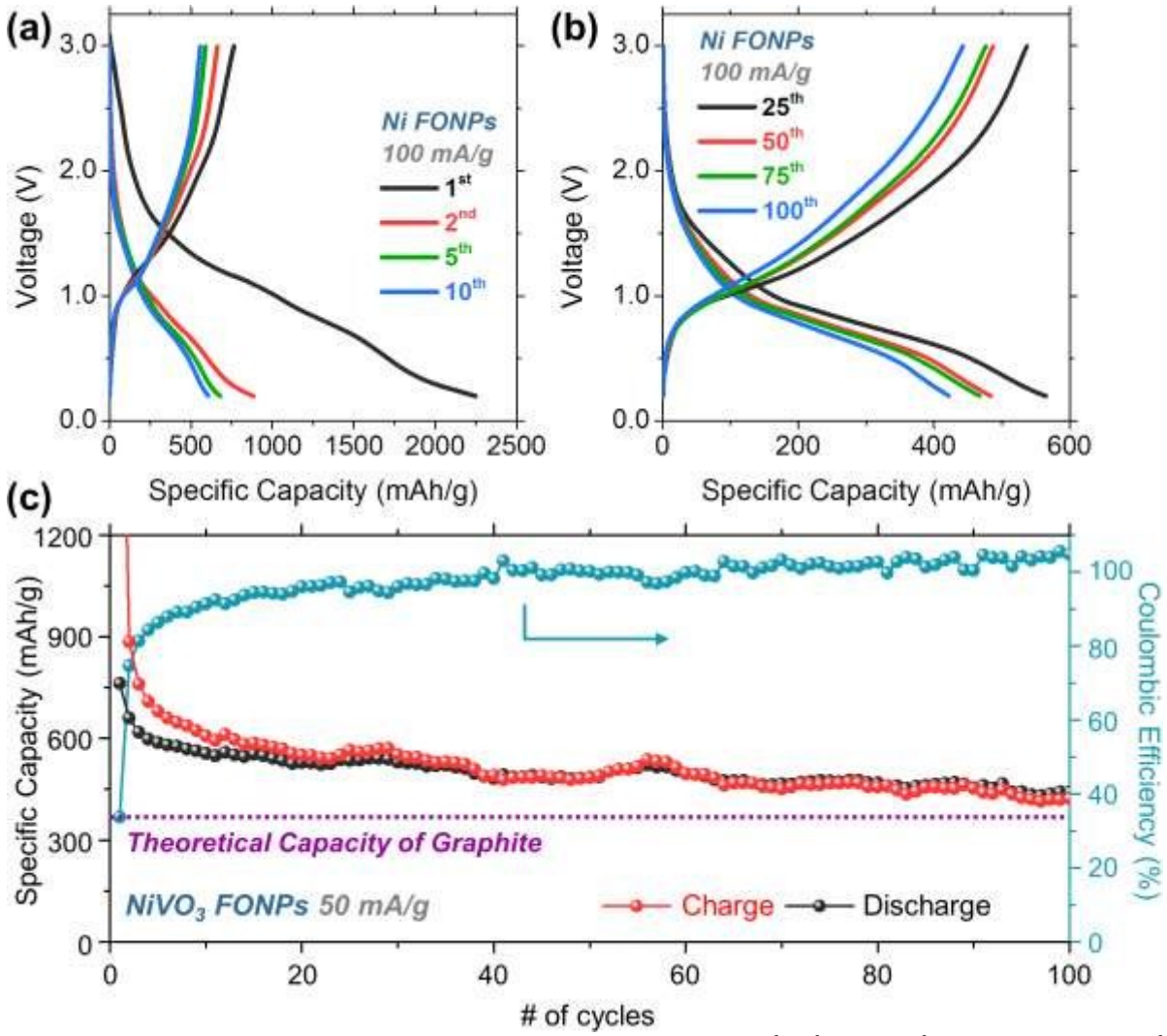


Fig. 6. Charge and discharge voltage profiles for (a) the 1st, 2nd, 5th and 10th cycles, (b) the 25th 50th, 75th and 100th for Ni-FONPs at a specific current of 50 mA/g in a potential window of 3.0 – 0.01 V (vs Li/Li^+). (c) Comparison of the specific capacity values and coulombic efficiency obtained for Ni-FONPs over 100 cycles.

Published on 28 August 2018. Downloaded by University College Cork on 9/6/2018 9:15:37 AM.

Journal of Materials Chemistry A Accepted Manuscript

View Article Online
DOI: 10.1039/C8TA05327H

Published on 28 August 2018. Downloaded by University College Cork on 9/6/2018 9:15:37 AM.

As discussed earlier, to our knowledge this is the first report on the electrochemical performance of $NiVO_3$, consequently there are no direct comparisons that can be drawn from the literature. There are reports on the electrochemical performance of various $Ni_3V_2O_8$ nanostructures [31, 33, 77-79], however not only are there differences in the stoichiometry of $NiVO_3$ and $Ni_3V_2O_8$, the two compounds also have significantly different crystal structures (triclinic and orthorhombic, respectively). Additionally, V present in $Ni_3V_2O_8$ is predominately in the V^{5+} oxidation state, whereas it is primarily present as V^{4+} in $NiVO_3$, as shown in the XPS analysis summarised in Table S2. Regardless of the differences in the crystal structure of $NiVO_3$ and $Ni_3V_2O_8$, the capacity values obtained for the Ni-FONPs are comparable to $Ni_3V_2O_8$, as listed in Table S3. The capacity values we observe for the $NiVO_3$ FONPs are also comparable to, and in some cases greater than, previously reported values for nanostructured V_2O_3 anodes, also shown in Table S3 and Fig. S9. Furthermore, galvanostatic cycling at 50 mA/g demonstrates that the $NiVO_3$ FONPs are capable of delivering capacities higher that the theoretical capacity of graphite (372 mAh/g for LiC_6).

4 Conclusions

Binary metal oxide $NiVO_3$ and composite Fe_2O_3/V_2O_3 fused oxide nanoparticles can be prepared directly from thermal treatment of Ni and Fe-doped vanadium oxide nanotubes. To our knowledge this is the first detailed report on the structural properties of $NiVO_3$, with only one previous report from 1970. Metal cation doped VONTs were then prepared via facile ion exchange reactions within the spacing between the scrolled crystalline layers of the VONTs, with salts of the respective metals. Recrystallization of transition metal cation doped VONTs resulted in two different materials form, but with suprisingly similar morphologies. Changes in the oxidation state of V before and after annealing, from XPS analysis, conclusively showed the formation of a single phase $NiVO_3$. On the other hand, thermal reduction of Fe doped

Journal of Materials Chemistry A Accepted Manuscript

View Article Online
DOI: 10.1039/C8TA05327H

VONTs did not result in the formation of a mixed Fe-V oxide, instead a composite of Fe_2O_3 and V_2O_3 was formed.

The mixed oxide Ni-FONPs significantly out performed the composite Fe-FONPs, in terms of both specific capacity values and capacity retention, when examined electrochemically as a Li-ion battery anode. The mixed composite of V_2O_3 and Fe_2O_3 exhibited capacity fading issues that are typical of conversion mode anode materials. Forming a single Ni-based vanadate completely removed capacity instability in early cycles and mitigated capacity fade during longer term cycling at fast and slow rates. This first report on the electrochemical performance of $NiVO_3$ is important as it identifies a synthetic route to Ni-containing high capacity anode materials directly from vanadium oxides, and avoids conversion mode reactions that are detrimental to anode stability. This anode material demonstrated exceptional specific capacities, achieving a reversible capacity of ~ 203 and 175 mAh/g after the 250^{th} and 500^{th} charges, respectively, when cycled with a specific current of 200 mA/g. The capacity retention of the Ni-FONPs from the 2^{nd} to the 500^{th} cycle was ~ 78%, which exemplifies their excellent capacity retention properties. Galvanostatic cycling at a slower rate further demonstated the electrochemical performance of the Ni-FONPs, achieving a large reversible capacity of ~ 420 mAh/g after 100 cycles, when cycled using a specific current of 50 mA/g. The electrochemical performance of the Ni-FONPs in terms of capacity retention, specific capacities and voltage stability over 500 cycles demonstrates that transmition metal vanadates, and possibly other oxides in a single phase form, function as anodes capacity-matched to most commonly used oxide cathodes and do so efficiently in binder-free and conductive additive-free electrode formulations. Furthermore, this particular oxide avoids conversion mode processes, significantly enhancing its stability for long cycle life Li-ion batteries.

Conflicts of interest

There are no conflicts to declare.

Published on 28 August 2018. Downloaded by University College Cork on 9/6/2018 9:15:37 AM.

Journal of Materials Chemistry A Accepted Manuscript

View Article Online
DOI: 10.1039/C8TA05327H

Acknowledgements

This work was supported by Science Foundation Ireland (SFI) through SFI Technology Innovation & Development Awards under contract no. 13/TIDA/E2761 and 15/TIDA/2893. This publication has also emanated from research supported in part by a research grant from SFI under Grant Number 14/IA/2581.

Published on 28 August 2018. Downloaded by University College Cork on 9/6/2018 9:15:37 AM.

Journal of Materials Chemistry A Accepted Manuscript

References

1. A. Mahmoudzadeh Andwari, A. Pesiridis, S. Rajoo, R. Martinez-Botas and V. Esfahanian, *Renew. Sust. Energ. Rev.*, 2017, **78**, 414-430.
2. L. Atzori, A. Iera and G. Morabito, *Comput. Netw.*, 2010, **54**, 2787-2805.
3. H. Gwon, J. Hong, H. Kim, D.-H. Seo, S. Jeon and K. Kang, *Energy & Environmental Science*, 2014, **7**, 538-551.
4. Y. Zhao, X. Li, B. Yan, D. Xiong, D. Li, S. Lawes and X. Sun, *Adv. Energy Mater.*, 2016, **6**, 1502175.
5. J. Yao, Y. Li, R. C. Massé, E. Uchaker and G. Cao, *Energ. Storage Mater.*, 2018, **11**, 205-259.
6. D. McNulty, D. N. Buckley and C. O'Dwyer, *J. Power Sources*, 2014, **267**, 831-873.
7. Y. Yue and H. Liang, *Adv. Energy Mater.*, 2017, **7**, 1602545.
8. Y. Dai, Q. Li, S. Tan, Q. Wei, Y. Pan, X. Tian, K. Zhao, X. Xu, Q. An, L. Mai and Q. Zhang, *Nano Energy*, 2017, **40**, 73-81.
9. P. Liu, K. Bian, K. Zhu, Y. Xu, Y. Gao, H. Luo, L. Lu, J. Wang, J. Liu and G. Tai, *ACS Appl. Mater. Interfaces*, 2017, **9**, 17002-17012.
10. Y. Zhang, Y. Wang, Z. Xiong, Y. Hu, W. Song, Q.-a. Huang, X. Cheng, L.-Q. Chen, C. Sun and H. Gu, *ACS Omega*, 2017, **2**, 793-799.
11. S. Gao, D. Zhang, K. Zhu, J. A. Tang, Z. Gao, Y. Wei, G. Chen and Y. Gao, *J. Alloys Compd.*, 2017, **702**, 13-19.
12. E. Armstrong, D. McNulty, H. Geaney and C. O'Dwyer, *ACS Appl. Mater. Interfaces*, 2015, **7**, 27006-27015.
13. J. Liu, H. Xia, D. Xue and L. Lu, *J. Am. Chem. Soc*, 2009, **131**, 12086-12087.
14. L. Zeng, C. Zheng, J. Xi, H. Fei and M. Wei, *Carbon*, 2013, **62**, 382-388.
15. X. Liu, Y. Hu, G. Jia, H. Zhang, H. Jiang and C. Li, *J. Mater. Chem. A*, 2016, **4**, 12030-12035.
16. L. Mai, L. Xu, C. Han, X. Xu, Y. Luo, S. Zhao and Y. Zhao, *Nano Lett.*, 2010, **10**, 4750-4755.
17. D. McNulty, Q. Ramasse and C. O'Dwyer, *Nanoscale*, 2016, **8**, 16266-16275.
18. X. Rui, J. Zhu, W. Liu, H. Tan, D. Sim, C. Xu, H. Zhang, J. Ma, H. H. Hng, T. M. Lim and Q. Yan, *RSC Adv.*, 2011, **1**, 117-122.
19. D. McNulty, D. N. Buckley and C. O'Dwyer, *ECS Trans.*, 2015, **64**, 1-12.
20. D. McNulty, D. N. Buckley and C. O'Dwyer, *RSC Adv.*, 2016, **6**, 40932-40944.
21. D. McNulty, D. N. Buckley and C. O'Dwyer, *ECS Trans.*, 2011, **35**, 237-245.
22. C. O'Dwyer, G. Gannon, D. McNulty, D. N. Buckley and D. Thompson, *Chem. Mater.*, 2012, **24**, 3981-3992.
23. J. M. Reinoso, H. J. Muhr, F. Krumeich, F. Bieri and R. Nesper, *Helv. Chim. Acta*, 2000, **83**, 1724-1733.
24. M. E. Spahr, P. Stoschitzki Bitterli, R. Nesper, O. Haas and P. Novák, *J. Electrochem. Soc.*, 1999, **146**, 2780-2783.
25. X. Zhou, G. Wu, G. Gao, J. Wang, H. Yang, J. Wu, J. Shen, B. Zhou and Z. Zhang, *J. Phys. Chem. C*, 2012, **116**, 21685-21692.
26. H. Kim, R.-H. Kim, S.-S. Lee, Y. Kim, D. Y. Kim and K. Park, *ACS Appl. Mater. Interfaces*, 2014, **6**, 11692-11697.
27. D. McNulty, D. Buckley and C. O'Dwyer, *J. Electrochem. Soc.*, 2014, **161**, A1321-A1329.
28. D. McNulty, D. N. Buckley and C. O'Dwyer, *J. Solid State Electrochem.*, 2016, **20**, 1445-1458.

View Article Online
DOI: 10.1039/C8TA05327H

Published on 28 August 2018. Downloaded by University College Cork on 9/6/2018 9:15:37 AM.

29. D. McNulty, D. N. Buckley and C. O'Dwyer, *ChemElectroChem*, 2017, **4**, 2037-2044.
30. A. R. Armstrong, C. Lyness, P. M. Panchmatia, M. S. Islam and P. G. Bruce, *Nat. Mater.*, 2011, **10**, 223.
31. C. Wang, D. Fang, H. e. Wang, Y. Cao, W. Xu, X. Liu, Z. Luo, G. Li, M. Jiang and C. Xiong, *Sci. Rep.*, 2016, **6**, 20826.
32. J. Xiang, X.-Y. Yu and U. Paik, *J. Power Sources*, 2016, **329**, 190-196.
33. B. Sambandam, V. Soundharrajan, J. Song, S. Kim, J. Jo, D. T. Pham, S. Kim, V. Mathew, K. H. Kim, Y.-K. Sun and J. Kim, *J. Electroanal. Chem.*, 2018, **810**, 34-40.
34. D. Deng, Y. Zhang, G. Li, X. Wang, L.-H. Gan, L. Jiang and C.-R. Wang, *Chem. Asian J.*, 2014, **9**, 1265-1269.
35. G. Yang, H. Cui, G. Yang and C. Wang, *ACS Nano*, 2014, **8**, 4474-4487.
36. H. J. Muhr, F. Krumeich, U. P. Schönholzer, F. Bieri, M. Niederberger, L. J. Gauckler and R. Nesper, *Adv. Mater.*, 2000, **12**, 231-234.
37. C.-J. Cui, G.-M. Wu, H.-Y. Yang, S.-F. She, J. Shen, B. Zhou and Z.-H. Zhang, *Electrochim. Acta*, 2010, **55**, 8870-8875.
38. S. Sharma, J. Thomas, A. Ramanan, M. Panthöfer and M. Jansen, *J. Nanosci. Nanotechnol.*, 2007, **7**, 1985-1989.
39. C.-j. Cui, G.-m. Wu, J. Shen, B. Zhou, Z.-h. Zhang, H.-y. Yang and S.-f. She, *Electrochim. Acta*, 2010, **55**, 2536-2541.
40. X. Chen, X. Sun and Y. Li, *Inorg. Chem.*, 2002, **41**, 4524-4530.
41. A. Dobley, K. Ngala, S. Yang, P. Y. Zavalij and M. S. Whittingham, *Chem. Mater.*, 2001, **13**, 4382-4386.
42. B. L. Chamberland, *J. Solid State Chem.*, 1970, **2**, 521-524.
43. B. L. Chamberland, *J. Solid State Chem.*, 1970, **1**, 138-142.
44. D. McNulty, D. N. Buckley and C. O'Dwyer, *ECS Trans.*, 2013, **50**, 165-174.
45. W. Chen, L. Q. Mai, J. F. Peng, Q. Xu and Q. Y. Zhu, *J. Mater. Sci.*, 2004, **39**, 2625-2627.
46. J. Liu, X. Wang, Q. Peng and Y. Li, *Adv. Mater.*, 2005, **17**, 764-767.
47. A. N. Mansour, *Surf. Sci. Spectra*, 1994, **3**, 231-238.
48. K. S. Kim and N. Winograd, *Surf. Sci.*, 1974, **43**, 625-643.
49. N. S. McIntyre and D. G. Zetaruk, *Anal. Chem.*, 1977, **49**, 1521-1529.
50. B. J. Tan, K. J. Klabunde and P. M. A. Sherwood, *Chem. Mater.*, 1990, **2**, 186-191.
51. G. Silversmit, D. Depla, H. Poelman, G. B. Marin and R. De Gryse, *J. Electron. Spectrosc. Relat. Phenom.*, 2004, **135**, 167-175.
52. Q. Wei, J. Liu, W. Feng, J. Sheng, X. Tian, L. He, Q. An and L. Mai, *J. Mater. Chem. A*, 2015, **3**, 8070-8075.
53. P. Jinshun, T. Seiji and K. Shigemi, *Jpn. J. Appl. Phys.*, 1998, **37**, 6519-6523.
54. C. V. Ramana, S. Utsunomiya, R. C. Ewing and U. Becker, *Solid State Commun.*, 2006, **137**, 645-649.
55. Y. Shi, Z. Zhang, D. Wexler, S. Chou, J. Gao, H. D. Abruña, H. Li, H. Liu, Y. Wu and J. Wang, *J. Power Sources*, 2015, **275**, 392-398.
56. B. Varghese, M. V. Reddy, Z. Yanwu, C. S. Lit, T. C. Hoong, G. V. Subba Rao, B. V. R. Chowdari, A. T. S. Wee, C. T. Lim and C.-H. Sow, *Chem. Mater.*, 2008, **20**, 3360-3367.
57. F. Lu, Q. Wu, X. Yang, L. Chen, J. Cai, C. Liang, M. Wu and P. Shen, *Phys. Chem. Chem. Phys.*, 2013, **15**, 9768-9774.
58. S. Zhu, M. Chen, W. Ren, J. Yang, S. Qu, Z. Li and G. Diao, *New J. Chem.*, 2015, **39**, 7923-7931.
59. X. Li, J. Fu, Z. Pan, J. Su, J. Xu, B. Gao, X. Peng, L. Wang, X. Zhang and P. K. Chu, *J. Power Sources*, 2016, **331**, 58-66.
60. Y. Sun, S. Jiang, W. Bi, C. Wu and Y. Xie, *J. Power Sources*, 2011, **196**, 8644-8650.
61. Y. Sun, X. Liu, F. Huang, S. Li, Y. Shen and A. Xie, *Mater. Res. Bull.*, 2017, **95**, 321-327.
62. K. E. Swider-Lyons, C. T. Love and D. R. Rolison, *Solid State Ion.*, 2002, **152–153**, 99-104.
63. H. Jiang, G. Jia, Y. Hu, Q. Cheng, Y. Fu and C. Li, *Ind. Eng. Chem. Res.*, 2015, **54**, 2960-2965.
64. X. Zhu, Y. Zhu, S. Murali, M. D. Stoller and R. S. Ruoff, *ACS Nano*, 2011, **5**, 3333-3338.
65. Y. Dou, J. Xu, B. Ruan, Q. Liu, Y. Pan, Z. Sun and S. X. Dou, *Adv. Energy Mater.*, 2016, **6**.
66. R. Wei, X. Zhou, T. Zhou, J. Hu and J. C. Ho, *J. Phys. Chem. C*, 2017, **121**, 19002-19009.
67. Z.-S. Wu, W. Ren, L. Xu, F. Li and H.-M. Cheng, *ACS Nano*, 2011, **5**, 5463-5471.
68. D. McNulty, H. Geaney and C. O'Dwyer, *Sci. Rep.*, 2017, **7**, 42263.

Journal of Materials Chemistry A Accepted Manuscript

69. D. McNulty, H. Geaney, E. Carroll, S. Garvey, A. Lonergan and C. O'Dwyer, *Mater. Res. Express*, 2017, **4**, 025011.
70. H. Geaney, D. McNulty, J. O'Connell, J. D. Holmes and C. O'Dwyer, *J. Electrochem. Soc.*, 2016, **163**, A1805-A1811.
71. D. McNulty, H. Geaney, E. Armstrong and C. O'Dwyer, *J. Mater. Chem. A*, 2016, **4**, 4448-4456.
72. Y. Li, L.-B. Kong, M.-C. Liu and L. Kang, *RSC Adv.*, 2016, **6**, 90197-90205.
73. V. Soundharrajan, B. Sambandam, J. Song, S. Kim, J. Jo, S. Kim, S. Lee, V. Mathew and J. Kim, *ACS Appl. Mater. Interfaces*, 2016, **8**, 8546-8553.
74. N. Yan, X. Zhou, Y. Li, F. Wang, H. Zhong, H. Wang and Q. Chen, *Sci. Rep.*, 2013, **3**, 3392.
75. L. Jiang, Y. Qu, Z. Ren, P. Yu, D. Zhao, W. Zhou, L. Wang and H. Fu, *ACS Appl. Mater. Interfaces*, 2015, **7**, 1595-1601.
76. B.-R. Jia, M.-L. Qin, Z.-L. Zhang, S.-M. Li, D.-Y. Zhang, H.-Y. Wu, L. Zhang, X. Lu and X.-H. Qu, *ACS Appl. Mater. Interfaces*, 2016, **8**, 25954-25961.
77. Y. Li, L.-B. Kong, M.-C. Liu, W.-B. Zhang and L. Kang, *Mater. Lett.*, 2017, **186**, 289-292.
78. C. Lv, J. Sun, G. Chen, C. Yan and D. Chen, *Nano Energy*, 2017, **33**, 138-145.
79. V. Soundharrajan, B. Sambandam, J. Song, S. Kim, J. Jo, D. T. Pham, S. Kim, V. Mathew and J. Kim, *Ceram. Int.*, 2017, **43**, 13224-13232.

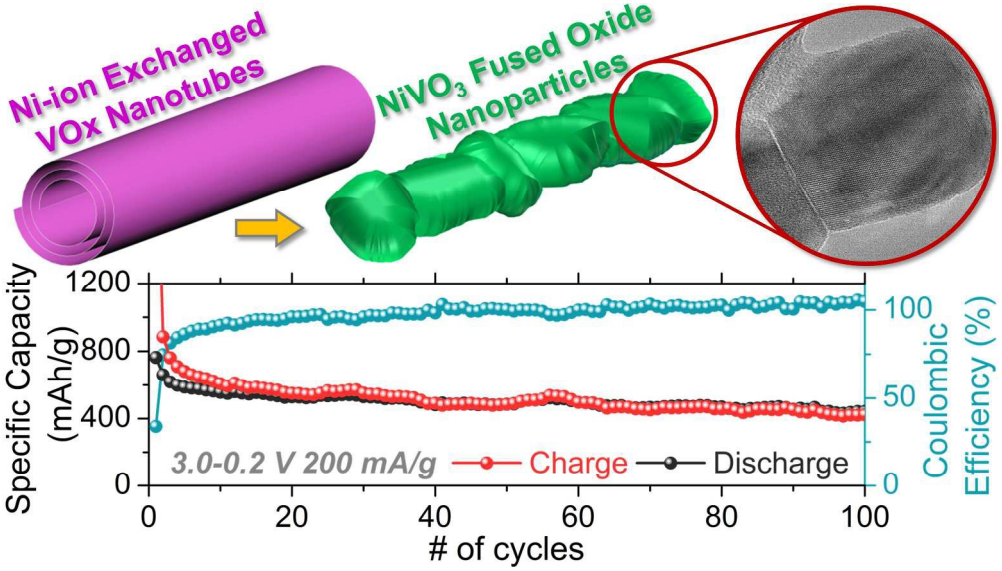
View Article Online
DOI: 10.1039/C8TA05327H

Published on 28 August 2018. Downloaded by University College Cork on 9/6/2018 9:15:37 AM.

Journal of Materials Chemistry A Accepted Manuscript

View Article Online
DOI: 10.1039/C8TA05327H

Published on 28 August 2018. Downloaded by University College Cork on 9/6/2018 9:15:37 AM.



254x143mm (300 x 300 DPI)

Journal of Materials Chemistry A Accepted Manuscript